Mitigating climate change and ozone pollution will improve Chinese food security

Shouxiu Li[1], Yang Gao[1*], Junxi Zhang[2], Chaopeng Hong[3], Shaoqing Zhang[4], Deliang Chen[5,6], Oliver Wild[7], Zhaozhong Feng[8], Yansen Xu[8], Xiuwen Guo[1], Wenbin Kou[1], Feifan Yan[1], Mingchen Ma[1], Xiaohong Yao[1], Huiwang Gao[1] and Steven J. Davis[9]

[1]Frontiers Science Center for Deep Ocean Multispheres and Earth System (FDOMES) and Key Laboratory of Marine Environmental Science and Ecology, Ministry of Education, Ocean University of China, and Laoshan Laboratory, Qingdao, 266100, China

[2]Zhejiang Lab, Hangzhou, 311100, China

[3]Institute of Environment and Ecology, Shenzhen International Graduate School, Tsinghua University, Shenzhen, 518000, China

[4]Key Laboratory of Physical Oceanography, Institute for Advanced Ocean Study, Frontiers Science Center for Deep Ocean Multispheres and Earth System (FDOMES), College of Oceanic and Atmospheric Sciences, Ocean University of China, Qingdao, 266100, China

[5]Department of Earth Sciences, University of Gothenburg, Gothenburg, 40530, Sweden

[6]Department of Earth System Sciences, Tsinghua University, Beijing 100080, China

[7]Lancaster Environment Centre, Lancaster University, Lancaster, LA1 4YQ, UK

[8]School of Ecology and Applied Meteorology, Nanjing University of Information Science & Technology, Pukou, Nanjing 210044, China

[9]Doerr School of Sustainability, Stanford University, Stanford, CA 94305, USA

*Correspondence: yanggao@ouc.edu.cn

Summary

Competition for land, partly driven by the trade-off between ensuring sufficient food production and expanding forest carbon sinks, intensifies the challenge of addressing climate change. This issue is further exacerbated by damage to plant stomata from ground-level ozone, reducing crop yields. Stomatal opening is regulated by meteorological processes that may change significantly under warming climate, but this effect has been largely overlooked in prior studies of crop ozone damage. Here, we show historical crop losses across China are 39 Tg annually, valued at roughly $15 billion. In a scenario where carbon emissions reach net zero in 2060, projected crop production losses could decline most, enough to provide an additional 80,000 calories per capita in China, or enabling a net absorption of 22 million tons of CO_2 annually through reverting surplus cropland to natural ecosystems. Our findings provide policy-relevant information to support continued efforts toward strict pollution control and climate mitigation.

Keywords: crop production, O_3, stomata, anthropogenic emissions, climate change

Introduction

Tropospheric ozone (O_3) is phytotoxic and detrimental to the growth of plants in both natural ecosystems and agricultural systems[1-4]. Given the importance of human food security[5-6], numerous studies have estimated the reductions in both the quantity and quality of agricultural crops resulting from ozone pollution. The impact of ozone on crops is strongly influenced by both its concentrations and meteorological conditions. These factors interact to determine the extent of ozone damage to crops, making their combined assessment essential for accurately capturing the overall impact on agricultural productivity[7-9].

Based on observed responses to cumulative exposure to ozone concentrations exceeding 40 ppb (a metric known as AOT40), it is estimated that ozone causes an annual crop production loss of 5-15% globally, resulting in economic losses of billions per year[10-16]. These losses are typically calculated based on reductions in crop yields and international market prices provided by FAOSTAT (Food and Agriculture Organization of the United Nations; www.faostat.org)[17-18]. The application of the same concentration metric suggests that recent ozone pollution in China has caused yield losses of 33%, 23%, and 9% for wheat, rice, and maize, respectively[19]. Other studies have used the AOT40 metric to project future ozone-induced crop losses, estimating decreases in global crop production between 2000 and 2030 of 5%-26% for wheat, 15%-19% for soybeans, and 4%-9% for maize under a scenario in which fossil fuel CO_2 emissions continue to increase[20]. Moreover, the increasing frequency of heatwaves under a warming climate is expected to exacerbate ozone pollution[21-23], leading to more severe crop losses. However, climate mitigation efforts may reduce both the frequency and intensity of heatwaves, thereby decreasing ozone concentrations and their adverse effects on crop yields. For instance, a recent study indicated that yields of perennial crops affected by ozone concentrations in California may increase by several percent in a lower warming scenario (RCP4.5 compared to RCP8.5)[24]. The reduced ozone levels in RCP4.5, as compared to RCP8.5, can be partially attributed to a weaker signal of meteorological changes, e.g., the smaller increase in near-surface air temperature under RCP4.5 suggests a reduced photochemical reaction rate relative to RCP8.5 (ref.[25-27]).

Meteorological conditions also play a critical role in plant physiology, particularly in transpiration rates and gas exchange at the leaf level. Damage to plants typically occurs when ozone molecules enter leaves through the stomata, a process that is highly sensitive to meteorological conditions, particularly the vapor pressure deficit (VPD). VPD is a measure of the drying power of the air and is often higher during periods of high ozone concentrations (because both are positively correlated with temperature and sunlight)[28-29]. However, high VPD periods tend to reduce ozone uptake in leaves, as stomata close to conserve water[30-32]. Neglecting these physiological processes and feedbacks may lead concentration-based metrics, such as AOT40, to substantially overestimate the impacts of ozone on crop production[33].

Here, we apply a novel process-based metric of ozone exposure that incorporates both meteorological and physiological factors—including stomatal conductance, vapor pressure deficit, soil moisture, and plant phenology—alongside ozone concentrations. This metric, known as the cumulative phytotoxic ozone dose above a flux threshold of y nmol O_3 m^{-2} s^{-1}(PODy)[3, 8, 11, 16, 34-38], offers a more sophisticated and representative measure of ozone impact. However, despite its advantages, PODy has been less frequently utilized compared to AOT40, as it depends on the plant-dependent ozone detoxification threshold (y) that varies with weather conditions and remains poorly characterized for many crops[8]. Recent experiments in China, employing both open-top chambers and free-air ozone concentration enrichment, have generated crop-specific values of y, making it possible to assess ozone impacts more accurately in China[39-42]. Notably, China accounts for 20% of the global production of wheat, maize, soybeans, and rice by mass[43-44] and has been experiencing increasing ozone levels for over a decade[45-48].

Further details of our analytical approach can be found in the Methods section. In brief, we evaluated ozone risks to key staple crops (winter wheat, rice, maize and soybean) in China during two periods: a historical baseline covering climate and pollution data from 2015 to 2019, and a future projection for 2056-2060 under the SSP126, SSP370, and SSP585 scenarios (SSP: Shared Socioeconomic Pathway[49]). Our analysis first disentangled the individual contributions of climate change and anthropogenic emissions to projected changes in ozone risks. The key assessment metric, PODy, was calculated using meteorological data from the Community Earth System Model (CESM), downscaled with the Weather Research and Forecasting (WRF) model, and combined with air pollution concentrations simulated by the WRF/CMAQ model. Our study explores how ozone exposure, modulated by meteorological conditions, may affect crop yields across China within the context of the nation's carbon neutrality goals.

Results

Annual crop yield losses attributable to ozone exposure in China during the historical period

Given that the widely adopted AOT40 index is still more commonly used than PODy, we initially applied AOT40 to estimate the relative yield loss. The response functions used to calculate crop production losses are provided in **Supplementary Table 1.** We compare our findings with previous research and contrast the results from the two metrics (**Fig. 1**). Since our simulation covers the 2015-2019 period, we selected studies from the same decade, i.e., 2010-2020, across China. The mean relative yield losses reported in these studies, based on AOT40, are 24%, 11%, 6%, and 8% for wheat, rice, maize, and soybean, respectively. The corresponding relative yield losses for these four crops in our study—28%, 17%, 8%, and 10%—are generally in line with the results from prior studies. The slightly higher relative yield loss for wheat observed in our study is consistent with findings from studies conducted in the latter half of the decade, specifically post-2015, with an average value of 28%. This increase likely reflects the rise in ozone concentrations in China in recent years[50].

Similar to previous research, our results show that the relative yield losses calculated using PODy are lower than those derived from AOT40 (**Fig. 1**). For example, in the studies by Feng et al.[51] and Wang et al.[52], the relative yield losses for wheat calculated using PODy are 7% and 5% lower, respectively, compared to those derived from AOT40 respectively. In our study, the relative yield losses for wheat, rice, maize, and soybean are 2%, 13%, 7%, and 6% lower than those calculated with AOT40, respectively. The yield losses for wheat and soybean reported in model simulations by Schauberger et al.[53] (**Fig. 1a,d**) are higher than those found in other studies.

AOT40 does not explicitly account for stomatal opening for ozone uptake flux, focusing solely on ozone exposure, with the underlying assumption that higher concentrations generally cause more significant crop damage[54-56]. By contrast, the PODy method directly accounts for stomatal ozone uptake, which is influenced by both ozone exposure and the degree of stomatal aperture[35, 56]. Meteorological conditions are key regulators of stomatal aperture and can strongly affect stomatal ozone uptake. As a result, PODy is considered a more suitable metric than AOT40 for assessing ozone-induced crop yield losses, particularly under evolving climate conditions. Therefore, we will primarily use the PODy metric for subsequent analyses. Detailed comparisons between the two metrics are provided in Section 1 of the supplementary information.

Fig. 2 shows the spatial distribution of estimated annual crop production losses across China due to ozone damage during the historical period, based on PODy, while the spatial distribution of relative yield losses is shown in Supplementary Fig. 3. Detailed calculations for these losses are described in the Methods section. Nationally, the ozone-induced crop losses are highest for wheat, totaling 26 Tg (26%), followed by rice (including double-early rice, single rice, and double-late rice) at 8 Tg (5%), maize at 3 Tg (1%), and soybean at 0.6 Tg (4%). The total crop losses for these four crops amount to 38 Tg/year, representing an economic loss of $15 billion, based on the annual purchase prices of crops during the historical period (https://www.fao.org/faostat/en/#data/PP, see Supplementary Table 2). To account for interannual variations in grain prices, we calculated the maximum and minimum economic losses using the highest and lowest purchase prices from the selected historical period, yielding values of \$17 billion and \$13 billion, respectively. These values deviate by less than 15% from the mean, indicating relatively modest interannual price fluctuations.

The significant regional differences in crop losses are primarily driven by variations in ozone uptake flux, which is affected by both ozone concentration and stomatal conductance (as detailed in the Methods section), along with crop production levels and species-specific ozone sensitivity. For example, major wheat-producing regions in central-eastern and North China are subject to more severe ozone pollution (**Supplementary Fig. 4**) than other agricultural areas. Additionally, wheat demonstrates higher sensitivity to ozone than other crops, which is reflected in its maximum stomatal conductance: 450 mmol O_3 m^{-2} PLA s^{-1} for wheat vs 370 mmol O_3 m^{-2} PLA s^{-1} for rice, 300 mmol O_3 m^{-2} PLA s^{-1} for soybean and 126 mmol O_3 m^{-2} PLA s^{-1} for maize. As a result, wheat suffers the greatest losses (**Fig. 2**), despite its annual production being lower than that of maize and rice (**Supplementary Fig. 5**).

However, for crops like maize and single rice, which show significant spatial variability in their primary production regions, differences in ozone concentration and stomatal conductance can lead to substantially different yield losses. To visualize the spatial variability in ozone concentration and stomatal ozone uptake rates (definition in Methods section) across each grid box, we normalize the anomalies of these two metrics for each grid box relative to the mean values of all grid boxes within the crop-growing region, using the standard deviation (**Supplementary Figs. 6 and 7**). For maize, primary production areas are in North China and the Northeast, with similar yields (**Supplementary Fig. 5**). However, due to much higher ozone concentrations in North China compared to the Northeast (**Supplementary Fig. 6**), and with comparable stomatal uptake rates (**Supplementary Fig. 7**), maize yield losses in North China are 3.6 times higher (**Fig. 2**). Similarly, single rice is mainly grown in central-southern and northeastern regions (**Supplementary Fig. 5**), and yield losses in the central-southern region are 5.7 times greater (**Fig. 2**), largely due to higher ozone levels (**Supplementary Fig. 6**).

Projected future changes in annual ozone-induced crop production losses

Future changes in crop production losses due to ozone uptake are primarily driven by shifts in air pollution emissions and meteorological conditions. To fully understand the impacts of ozone precursors and climate change on future ozone-induced crop production losses, we calculated the changes in crop production relative to the historical period following the Shared Socioeconomic Pathways SSP126, SSP370, and SSP585 (**Fig. 3a**). Additionally, we discuss the production of different crops, along with the cumulative probability distribution of ozone concentration and stomatal ozone uptake rates, in Section S2 of the supplementary information. Furthermore, we conducted three additional numerical sensitivity experiments ($E_{hist}M_{126}$, $E_{hist}M_{370}$ and $E_{hist}M_{585}$) where emissions are held constant at historical levels while climate follows the SSP126, SSP370, and SSP585 pathways. This approach allows us to isolate the contributions from changes in emissions (SSP126-$E_{hist}M_{126}$; SSP370-$E_{hist}M_{370}$; SSP585-$E_{hist}M_{585}$) and climate change ($E_{hist}M_{126}$-Hist; $E_{hist}M_{370}$-Hist; $E_{hist}M_{585}$-Hist). More detailed information can be found in the Methods section.

The annual crop production for the four crops during the historical period is 537 Tg, with 101 Tg (19%), 224 Tg (42%), 15 Tg (3%), and 197 Tg (36%) for wheat, maize, soybean, and rice respectively (https://www.stats.gov.cn/). **Fig. 3** illustrates the ozone-induced crop production change relative to the historical period for different crops under various future scenarios**.** Under the combined effects of a changing climate and emissions, overall crop production increases relative to the historical period, with an increase of 38 Tg in SSP126 and 6 Tg in SSP585, but a decrease of 14 Tg in SSP370 (Total_net in **Fig. 3a)**. Notably, the benefits of crop production in SSP126 are six times greater than those in SSP585, highlighting the advantages of pursuing carbon neutrality for food security.

By isolating the contributions of emissions and climate change, we find that the main driver behind the increased crop production under the SSP126 scenario is the significant reduction in anthropogenic emissions, accounting for over 90% of the increase in crop production (pink in **Fig. 3a**). The impact of air pollutant emissions on crop production losses is primarily driven by changes in ozone concentration. Under SSP126, the reduction in ozone precursors leads to substantial decreases in ozone concentrations (Supplementary **Fig. 9a-d**) and a corresponding reduction in ozone uptake flux. In contrast, the elevated ozone concentrations resulting from increased anthropogenic emissions under the SSP370 scenario are the primary driver of decreased crop production (**Fig. 3a**).

The influence of meteorological conditions can be decomposed into three components: the effect of ozone concentrations resulting from changes in meteorology (Climate_O_3; solid purple in **Fig. 3a**), the effect of meteorology on stomatal ozone uptake rate (Climate_Met; dotted purple in **Fig. 3a**), and the combined effect of changes in both ozone and meteorology (Nonlinear effect; dashed purple in **Fig. 3a**). This nonlinearity represents the interactions between these terms (Climate_O_3 and Climate_Met) and is defined as the perturbation term for simultaneous changes in ozone concentration and meteorological conditions (see Methods section—Model configurations and dynamical downscaling technique). The impact of climate-induced ozone concentrations on crop production under climate change is negative, and this negative effect is smaller under SSP585 and SSP370 than under SSP126, due to a stronger increase in ozone concentrations under SSP126. While higher near-surface temperatures in SSP585 and SSP370 compared to SSP126 (**Supplementary Fig. 10**) favor enhanced ozone concentrations, an additional increase in water vapor at 2 m under SSP585 and SSP370 (**Supplementary Fig. 11**) may act as an ozone sink and partly mitigate ozone concentration increases[57].

In addition to the effects of climate on ozone, changes in meteorological conditions under a warming climate play an important role in modulating ozone uptake, particularly by influencing stomatal conductance and the rate of photosynthesis[30-31, 58]. The combined effects result in a positive impact on crop production (dotted purple in **Fig. 3a**), yielding an extra crop production of 7.39 Tg in SSP126, 4.08 Tg in SSP370 and 5.27 Tg in SSP585, which offsets most of the crop losses from the climate-induced ozone increase, 9.91 Tg in SSP126, 8.21 Tg in SSP370 and 7.18 Tg in SSP585 (solid purple vs. dotted purple in **Fig. 3a**). Moreover, a nonlinear interaction exists between the effects of climate on ozone and stomatal ozone uptake rate (dashed line in **Fig. 3a**), which could enhance crop production by 1.69 Tg, 1.97 Tg and 1.57 Tg under SSP126, SSP370, and SSP585, respectively. This effect diminishes the extent of stomatal uptake when future ozone concentrations increase due to rising temperatures in a warming climate. Thus, future meteorological constraints on stomatal uptake could mitigate crop losses caused by elevated ozone.

The increase in crop production underscores the prospects for an increased food supply. Under SSP126 and SSP585, increased crop production could lead to additional annual per capita gains of 26 kg and 4 kg of grains, respectively, in China. This estimate is based on the increased crop production (black dot in **Fig. 3a**) and the average annual population from the historical period (https://www.stats.gov.cn/). Based on the calorific value of staple crops (**Supplementary Table 3**; https://www.fao.org/3/X9892E/X9892e05.htm), we calculated that the incremental gains under SSP126 and SSP585 could provide an additional 238 and 34 kcal/day respectively per capita (**Fig. 3b**). In contrast, reduced crop production in SSP370 may induce a decrease of 87 kcal/day per capita annually (**Fig. 3b**). These results highlight improved food security under low-emission scenarios.

Beyond food security concerns, achieving carbon neutrality is a major challenge for both China and the world[59-60]. Forest carbon sequestration remains the most cost-effective natural method for reducing atmospheric CO_2 (ref.[61]). Based on the estimated annual grain yield (6098 kg/ha; https://www.stats.gov.cn/), the reduction in crop production losses under SSP126 is equivalent to the crops grown on 6 million hectares (Mha) of farmland. If this farmland were fully reforested, it would increase China's total forest area by 3% (https://www.stats.gov.cn/). Given that China currently has 200 Mha of forest, capable of sequestering 670-870 million tons of CO_2 (ref.[62]), this additional reforested area would capture an extra 22 million tons of CO2 annually (**Fig. 3b**).

Reduced crop production losses due to weaker ozone uptake

Extreme weather events substantially influence ozone concentrations[26, 63] and stomatal conductance[64], which in turn affect ozone-induced crop production losses. To explore how these events impact ozone uptake flux in crops, we examined daily mean ozone concentrations and ozone uptake fluxes during both heatwave and non-heatwave periods throughout the phenological cycle of wheat in the historical period (Fig. 4).

Our results show that while ozone concentrations are, on average, 20% higher during heatwaves, the PODy is considerably lower during heatwaves compared to non-heatwave conditions (**Fig. 4a**). Since ozone absorption flux is jointly determined by ozone concentration and stomatal uptake rate, we analyzed the relative yield loss in relation to these two metrics (**Fig. 4b**). The results show a notable interaction between ozone concentration and stomatal ozone uptake rate, which together modulate ozone-induced relative yield loss. Additionally, ozone uptake flux is substantially reduced under low stomatal ozone uptake rates. Therefore, the lower PODy during heatwaves is attributed to a marked reduction in stomatal ozone uptake rate (**Fig. 4a**), despite higher ozone concentrations. Specific meteorological conditions during heatwaves may limit stomatal uptake.

Our analysis identifies the key limiting factor for reduced stomatal ozone uptake as the high vapor pressure deficit (VPD) during heatwaves (**Fig. 4c**, **Supplementary Figs. 12-13**). This is further illustrated in **Fig. 4d**, where stomatal ozone uptake rates initially increase with rising VPD but decline at higher VPD levels, underscoring the role of optimal atmospheric water availability in controlling stomatal closure. However, uncertainties persist due to the complex relationship between VPD, stomatal ozone uptake rate, and relative yield loss (**Fig. 4d**). Process-based simulations may help elucidate the underlying mechanisms.

Discussion

Ozone pollution poses a significant threat to crop yields, particularly in China, due to the country's large-scale agricultural production and the escalating severity of recent ozone pollution. The effect of ozone on crop production is determined not only by ozone concentrations but also by the extent of ozone uptake by crops, which is heavily influenced by meteorological conditions. While previous studies of ozone-induced crop losses have primarily focused on changes in ozone concentrations, the PODy index used here incorporates the sensitivity of plant physiology to meteorological conditions, which tends to moderate ozone-related crop losses. By considering future SSP585, SSP370, and SSP126 scenario pathways, we find that under SSP370, annual crop production decreases by 14 Tg by mid-century. In contrast, there is an increase of 6 Tg under SSP585, and an additional 38 Tg under SSP126. The surplus grain under SSP126 would provide an additional 238 kcal/day per capita annually. As these extra calories would exceed domestic demand, food prices in China could be expected to decrease, potentially leading to increased grain exports or more livestock feed. Alternatively, if total grain production were maintained and surplus land were reforested, net carbon uptake by such forests could reach roughly 22 million tons of CO_2 annually, contributing to China's efforts to achieve carbon neutrality and mitigate future temperature increases[65-67]. The reduction in anthropogenic emissions plays a crucial role in achieving increased production under a low-emission scenario, highlighting that continued ambitious emission reduction efforts will significantly enhance China's food security. However, changes in stomatal uptake should not be overlooked under strong climate warming, as the positive effects from reduced stomatal uptake driven by meteorological conditions outweigh the negative effects of increased ozone concentrations on crop yields.

Our findings are subject to several important uncertainties and limitations. First, the detoxification threshold y is a key factor in PODy, representing the plant's capacity to detoxify ozone. Only ozone fluxes exceeding this threshold are assumed to cause damage to crops. In this study, a fixed detoxification threshold was used. However, crops exhibit differences in their adaptation and detoxification capacities at various developmental stages[68-72]. For example, Wu et al.[73] considered dynamic detoxification thresholds that vary with the time of day and the growth stages of winter wheat, expressed as a function of the gross photosynthesis rate. They found that these flux thresholds fluctuate daily, peaking between the flowering and grain filling stages. Although we used a fixed threshold, the fitting process between PODy and crop yield accounts for the varying responses of crops to ozone at different growth stages. This is why a fixed threshold is commonly employed in most studies[40, 74-77]. Future research could focus on developing dynamic detoxification thresholds to further investigate their impact on crop yield.

Second, we did not account for changes in land cover, which is a key driver of climate change[78-82], and affects agricultural productivity[83]. For instance, the agricultural land area is projected to decrease by approximately 4% by the end of the century under SSP126 (ref.[84]), which could influence future crop projections[85-88]. Third, our conclusions are based on five-year simulations conducted using a single model. While our model represents over a decade of refinements, including improvements in land use, land cover, and eddy diffusivity[89-90], as well as bias corrections due to boundary layer effects[91-92], multi-model ensembles hold the potential to further reduce uncertainties. Similarly, while decadal simulations might better capture climate conditions, our previous systematic analysis indicated that five-year periods are representative for climate change studies (Supplementary Figs. 5-8 in ref.[93]).

In the context of future projections, phenology was primarily calculated based on simulated future conditions, with the exception of the flowering date, which remains consistent with historical periods due to data limitations. This approach introduces uncertainties. For instance, between 1986 and 2011 in China, the flowering date for spring crops, including winter wheat, rice, and spring maize, advanced by approximately 0.23 ± 0.47 days per year[94-95] due to warming trends. Assuming the relationship between flowering date and temperature holds in the future, the flowering date is expected to shift slightly earlier. To address this uncertainty, we conducted a sensitivity test by advancing the flowering date by 1, 3, and 5 days to assess its impact on ozone-related crop losses. The results showed that variations in crop loss due to ozone under future warming scenarios were within 4%, indicating that crop loss is only marginally sensitive to changes in the flowering date (**Supplementary Table 7**).

Several studies have shown that ozone can reduce the relative grain number per ear and the relative single grain weight, both of which impact overall crop yield[96]. Ozone also affects crop quality, influencing starch, protein, nutrient, and oil content. For instance, ozone reduces starch content while increasing the protein and nutritional content of crops such as wheat and rice[97-98]. This study does not account for these effects, but future research could further investigate the combined impacts of climate and ozone on both crop yield and quality. Such work would provide deeper insights into yield composition under varying environmental conditions.

Despite these uncertainties, our results suggest that climate mitigation efforts in China will substantially reduce ozone-related crop losses. Policymakers should thus consider food security and the more efficient use of land and agricultural inputs as additional benefits of transitioning toward carbon neutrality. Although this study focuses on China, there is good reason to believe that similarly substantial increases in crop yields could occur in other agricultural regions worldwide if the global climate goals are achieved.

Data and methods

Study areas and crops. The geographical scope of this study is limited to mainland

China, excluding Hong Kong, Macao, and Taiwan. Four major types of crops are selected, including winter wheat (hereinafter referred to as wheat), rice, maize, and soybean. It is important to note that spring wheat is excluded from this analysis, as it constitutes only about 5% of the total wheat production (https://www.stats.gov.cn/). Wheat is predominantly grown in the central-eastern and North China. According to the crop cycle and growing seasons, rice can be categorized into three types: single rice, double-early rice, and double-late rice. Single rice, planted and harvested once a year, has a growth period mainly concentrated from July to September across China. Double-season rice is planted and harvested twice within a single calendar year. The crop with a growth period between May and July is referred to as double-early rice, while the one with a growth period between August and October is known as double-late rice. Maize is cultivated in most areas of China, primarily in the North China and Northeast regions, while soybean cultivation extends to all provinces except Hainan and Qinghai (**Supplementary Fig. 5**).

Model configurations and dynamical downscaling technique. The Community Earth System Model (CESM) version 2.1.3 is used to provide initial and boundary conditions for a regional air quality model, based on the Weather Research and Forecasting Model version 3.8 (WRF3.8) and the Community Multi-scale Air Quality Model version 5.2 (CMAQ5.2) for both historical and future periods. In CESM, the atmospheric component uses the Community Atmosphere Model (CAM) for simulations, with the Whole Atmosphere Community Climate Model (WACCM) selected for atmospheric chemistry mechanisms. The spatial resolution of the atmospheric component of CESM is 0.9° × 1.25°, which is subsequently downscaled to a finer resolution in WRF/CMAQ using a dynamical downscaling approach[25]. In this study, CESM outputs are dynamically used to establish boundaries for the outer WRF/CMAQ domain for high-resolution regional simulations (**Fig. 5**). The dynamical downscaling tool was developed in our previous study[29]. The downscaling process involves both meteorological and chemical composition downscaling, along with horizontal and vertical interpolations. For meteorological downscaling, 6-hourly meteorological variables—such as temperature (T), wind components (U, V), relative humidity (RH), and geopotential height (GHT)—output from CESM are dynamically interpolated to provide initial and boundary conditions for WRF simulations. For chemical composition downscaling, the initial step involves mapping chemical species from CESM to CMAQ, addressing differences in chemical mechanisms and species representation between the two models. The mapping table can be found in a previous study[25]. The mapped chemical species concentration data, provided at a 6-hourly resolution, is then used to establish initial and boundary conditions for CMAQ. The ozone concentration and meteorological factors output from the regional model are subsequently used to calculate ozone uptake flux and ozone-induced crop production losses.

The grid spacing of WRF/CMAQ is set at 36 km × 36 km with 34 vertical layers extending up to 50 hPa. The modeling domain for both WRF and CMAQ is centered at 34° N, 110° E, encompassing all of China as well as several surrounding countries and regions. In CMAQ, we utilize the CB06 gas-phase chemical mechanism[99] and the AERO6 aerosol mechanism[100] to simulate the transformation of gases and aerosol species in the atmosphere. Additional details regarding the configuration can be found in Supplementary Table 4. The ozone concentration and meteorological factors output from the regional model are used to the calculation of ozone uptake flux and ozone-induced crop production losses, with further details provided in the following section.

In CESM, the anthropogenic emissions are derived from the global emission data produced by the Community Emissions Data System (CEDS) released for CMIP6 (https://esgfnode.llnl.gov/projects/input4mips), covering the years 1750 to 2100. For CMAQ, the anthropogenic emissions over China during the historical period are based on the Multi-resolution Emission Inventory (MEIC) released by Tsinghua University (http://www.meicmodel.org). Future anthropogenic emissions for China are scaled according to the ratio of national emissions under the SSPs to that during the historical period[92]. Hourly biogenic emissions are calculated using the Model of Emissions of Gases and Aerosols from Nature version 2.1. Emission inventories for biomass burning and shipping are sourced from the Global Fire Emissions Database Version 4 (GFED V4)[101] and the Shipping emission inventory model (SEIM)[102], respectively.

Numerical simulations for the period of 2015–2019 are designated as the historical simulation (referred to as Hist), while the future period under the SSP scenarios is set for 2056-2060. Since the starting year for the SSPs is defined as 2015, the first five-year period from SSP245 is used for the Hist scenario. It is assumed that the differences between the SSP scenarios during these initial five years are minimal, and do not affect the conclusions drawn in this study. For the future periods, simulations are carried out following the sustainability pathway SSP126, a low-emission scenario broadly representative of the transition toward carbon neutrality, as well as the regional rivalry pathway SSP370 and the fossil fuel-intensive pathway SSP585. All these future scenarios entail a degree of climate warming. In addition, we conduct three more numerical sensitivity experiments for the future period in which emissions are maintained at historical levels while the climate follows the SSP126, SSP370 and SSP585 pathways. These scenarios, referred to as $E_{hist}M_{126}$, $E_{hist}M_{370}$ and $E_{hist}M_{585}$, are intended to isolate the effects of anthropogenic emissions and climate change on future ozone-induced changes in crop production.

By comparing the SSP simulations (SSP126: $E_{126}M_{126}$; SSP370: $E_{370}M_{370}$; SSP585:

$E_{585}M_{585}$) with their corresponding sensitivity experiments ($E_{hist}M_{126}$, $E_{hist}M_{370}$, and $E_{hist}M_{585}$), we can isolate the effects of emissions, such as by comparing $E_{126}M_{126}$ with $E_{hist}M_{126}$. Additionally, by contrasting the numerical experiments with historical simulations (e.g., $E_{hist}M_{126}$ vs. $E_{hist}M_{hist}$), the differences reflect the impact of climate change on yield loss. The changes in crop production losses can be broken down into three components: the effect of meteorology on stomatal ozone uptake rates, the effect of ozone concentrations driven by meteorological changes, and the combined (synergistic) impact of changes in both ozone and meteorology.

To clarify these components, we developed the diagram presented below (**Fig. 6**). In the historical period (Hist: $E_{hist}M_{hist}$), we represent ozone concentration as x_1, meteorological conditions as m_1, and crop production losses as y_1. In the future period (using SSP126 with historical emissions as an example: $E_{hist}M_{126}$), we denote the ozone concentration as x_2, meteorological conditions as m_2, and crop production losses as y_2. Considering the joint regulatory effects of meteorological conditions and ozone concentration on crop yield, we propose that their product determines crop production losses, expressed as $y_1 = x_1 m_1$ and $y_2 = x_2 m_2$. Therefore, the change in crop production losses due to meteorological changes (y_2-y_1) can be derived from the formula in the diagram below. This formula captures the impact of changes in ozone concentrations due to meteorology ($m_1(x_2$-$x_1)$), the effect of meteorology on stomatal ozone uptake rate ($x_1(m_2$-$m_1)$), and the nonlinear interactions between ozone and meteorology ($(m_2$-$m_1)(x_2$-$x_1)$).

Ozone metrics utilized in this study. The PODy metric quantifies ozone damage accumulated over the crop's growing period during daytime when surface radiation exceeds 50 W/m^2, coinciding with stomatal fluxes of O_3 rises surpassing a specified threshold. The thresholds used for wheat, rice, maize and soybean is 12 nmol O_3 m^{-2} s^{-1} (ref.[40]), 9 nmol O_3 m^{-2} s^{-1} (ref.[39]), 6 nmol O_3 m^{-2} s^{-1} (ref.[41]) and 9.6 nmol O_3 m^{-2} s^{-1} (ref.[42]) respectively. The temperature dependent phenological data for crops used in this study are sourced from research conducted in China[103-104]. Determining the phenological period requires identifying the start and end dates based on the flowering date and effective temperature sums. The flowering date corresponds to mid-anthesis, defined as five days after the heading date[96]. For the historical period, heading dates are available for wheat, rice, and maize at a 1 km grid level[103] and for soybean at the provincial level[104]. Once the flowering date is established, we identify two intervals—before and after the flowering date—where the accumulated effective temperature reaches specific thresholds (e.g., 200°C before and 600°C after flowering date for wheat[40]). The effective temperature is defined as the daily average temperature conducive to crop growth (e.g., for wheat, daily averages above 0°C). The time span between these dates marks the active growth phase of crops, when they are particularly sensitive to ozone[1]. Impacts on crops were estimated within this growth period. Incorporating phenology helps account for crop growth rates, as the length of the growth period tends to negatively correlate with temperature. We have factored in the effect of temperature on the growth period by evaluating effective accumulated temperature during both historical and future periods. Across the three climate scenarios (SSP126, SSP370, SSP585), the phenological period for all crops in this study is projected to shorten by an average of 5% to 10% compared to historical periods.

The stomatal flux of O_3 (F_{sto}: in nmol O_3 m^{-2} s^{-1}), is calculated following the approach recommended by the Convention on Long-Range Transboundary Air Pollution (LRTAP)[1]:

$$F_{sto} = [O_3] \times \frac{1}{r_b + r_c} \times \frac{g_{sto}}{g_{sto} + g_{ext}} \tag{1}$$

where $[O_3]$ is the ozone concentration in nmol m^{-3} at canopy height. The ozone concentration in the lowest layer of the model, representing a height of approximately 15~20 m, is scaled to the canopy height (e.g., 1m for wheat, rice, and soybean, 2 m for maize) by applying a factor of 0.9 (ref.[1]). g_{ext} is the external leaf or cuticular conductance, set to a fixed value of 0.0004 m s^{-1} (ref.[1]). The fraction of this O_3 taken up by the stomata is given by gsto/(gsto+gext). Therefore, the physical interpretation of the term 1/(rb+rc)×gsto/(gsto+gext) represents the stomatal ozone uptake rate (m s^{-1}). Here, r_b denotes the leaf boundary layer resistance (s m^{-1}) and r_c represents the canopy resistance (s m^{-1}). These resistances are calculated as follows:

$$r_b = 1.3 \times 150 \times \sqrt{\frac{L}{u}} \quad (2)$$

$$r_c = \frac{1}{g_{sto} + g_{ext}} \quad (3)$$

where L is the leaf width, set at 0.02 m, and u is the wind speed (m s^{-1}) at the canopy height. The constant 150 has units of $s^{1/2}$ m^{-1}, while the factor of 1.3 adjusts for the differences in diffusivity between heat and O_3. The g_{sto} represents the stomatal conductance of ozone (mmol O_3 m^{-2} s^{-1}) and is central to the calculation of leaf ozone flux, as it reflects the magnitude of stomatal aperture. This is calculated based on the Eq. 4 (ref.[105-106]).

$$g_{sto} = g_{max} \times \min(f_{phen}, f_{O3}) \times f_{light} \times \max(f_{min}, (f_{VPD} \times f_{temp} \times f_{PAW})) \quad (4)$$

where the formulation generally consists of two components: maximum stomatal conductance (g_{max}) and various modifying parameters that reflect the influence of phenology (f_{phen}), ozone concentration (f_{O3}), and four environmental variables— light (irradiance, f_{light}), atmospheric water vapor pressure deficit (VPD, measured as f_{VPD}), 2-meter air temperature (f_{temp}),and soil water availability (f_{PAW} , indicating the potential available water content). f_{min} is the relative minimum stomatal conductance that occurs during daytime, and is a constant determined by the ratio of the minimum stomatal conductance to the maximum stomatal conductance.

These modifying parameters are expressed in relative terms (i.e., values between 0 and 1) as proportions of g_{max} and the equations governing them for each crop are taken from previous studies[39-42]. The values of f_{phen} and f_{O3} represent the effects of normal aging and ozone-induced premature senescence on stomatal function, respectively, with the smaller value of the two being used, as it has a greater impact on stomatal conductance. The f_{light} is a function of photosynthetic photon flux density and represents the control of incoming solar radiation on stomatal aperture. The term $\max(f_{\min}, (f_{VPD} \times f_{temp} \times f_{PAW}))$ represents the synergistic effects of atmospheric water vapor pressure deficit, temperature, and soil water content on stomatal conductance, ensuring that the value does not fall below the $f_{\min}$, the relative minimum stomatal conductance. The soil water content f_{PAW} is closely linked to irrigation practices, and the impact of irrigation on ozone-induced crop production losses is discussed in detail in Section 3 of the supplementary information.

Each modifying parameter influences stomatal conductance in different ways. In general, stomatal conductance rapidly increases with light levels, reaching a maximum at relatively low intensities and then stabilizing despite further increases in light[107-109]. In contrast, the effects of temperature and humidity on stomatal conductance are more complex and variable, depending on plant species and other contributing factors[110-111]. By incorporating these factors, we accounted for the stomatal response to meteorological conditions and ozone levels. The g_{sto} from Eq. 4 is converted from units of mmol O_3 m^{-2} s^{-1} to m s^{-1} by dividing by 41000 (ref.[1]) for application in Eq. 1. The calculated stomatal conductance values were validated against observed values, demonstrating strong agreement for winter wheat[40], maize[41], rice[39] and soybean[42].

In addition to the PODy metric, the standard AOT40 metric is evaluated for comparison. AOT40 (measured in ppm h) represents the accumulated hourly ozone concentrations above 40 ppbv between 8:00 AM and 8:00 PM (local standard time) during the crop growing period (Supplementary Table 5), which is defined here as three consecutive months[112-114]. The hourly model surface ozone concentration is scaled to canopy height using a factor of 0.9, as previously mentioned (ref.[1]).

Evaluation of ozone concentration. We achieved reasonable model performance by comparing multiyear mean daily ozone observations with model output across China during the historical period (2015-2019; **Supplementary Fig. 16**). The ozone observations were sourced from the Ministry of Ecology and Environment of the People's Republic of China (https://www.mee.gov.cn). Overall, the performance meets the benchmarks for mean fractional bias (MFB) and mean fractional error (MFE), which are set at 15% and 35%, respectively[115].

Estimation of relative yield loss. The crop response to ozone is obtained through linear regression analysis of crop yield against selected ozone metrics. The response functions that calculate the relative yield (RY, %) for each crop based on PODy and AOT40 are provided in Supplementary Tables 6 and 1, respectively. The relative yield loss (RYL, %) is defined as one hundred minus the relative yield.

Estimation of O_3-induced crop production losses and economic cost loss. Based on the results of relative yield loss, the crop production loss (CPL) is then obtained according to the following equation:

$$CPL = CP \times \frac{RYL}{100 - RYL} \tag{5}$$

where CP represents the annual crop production at the provincial level from 2015 to 2019, as proved by the National Bureau of Statistics (NBS; http://www.stats.gov.cn/). The national crop production data is subsequently mapped onto the model grid, which has a resolution of 36 km × 36 km. The fractional coverage of each crop is defined as follows[116].

$$f_{crop_i} = f_{cropland} \times \left(\frac{crop_i}{cropland}\right) \quad (6)$$

where f_{crop_i} is the fractional coverage of the specific crop i in a grid cell, calculated as the proportion of cropland in the grid cell, $f_{cropland}$, scaled by the proportion of cropland area devoted to that crop at the provincial level. $f_{cropland}$ is obtained from the spatial cropland dataset GAZE 2000 (https://sedac.ciesin.columbia.edu/data/set/aglands-croplands-2000/), $crop_i$ is the provincial area for the specific crop i, and $cropland$ encompasses the total cropland area in each province (**Supplementary Fig. 17**; http://www.stats.gov.cn/).

The economic cost losses (ECL) are calculated according to the crop production losses and the annual international purchase prices. The purchase prices for each crop from 2015 to 2019 are sourced from FAOSTAT (https://www.fao.org/faostat/en/#data/PP), and are detailed in **Supplementary Table 2**.

Definition of the heatwaves. In this study, we define the temperature threshold for heatwave events based on the optimal growth temperature for crops. Given that winter wheat in China suffers the most significant yield loss due to ozone damage, we use it as a case study to assess the impact of ozone on yield loss during heatwaves. The optimal growth temperature for winter wheat is 26°C[1]. Therefore, we define a heatwave as a period when the daily average temperature consistently exceeds 26°C for three consecutive days. The evaluation of heatwave duration during the phenological period of wheat, based on the fifth generation ECMWF atmospheric reanalysis of global climate (ERA5) and WRF, is illustrated **Supplementary Fig. 18**, showing strong consistency between model outputs and ERA5. For example, approximately 30% of days exceed this threshold in the major wheat production area of the North China Plain (**Supplementary Fig. 19**).

Acknowledgment

This work was supported by the National Natural Science Foundation of China (42122039, 42375189), Fundamental Research Funds for the Central Universities (202341001, 202261069). We acknowledge the High Performance Computer resources (2024-EL-ZD-000146, 2023-EL-ZD-000104) from the National Key Scientific and Technological Infrastructure project "Earth System Numerical Simulation Facility" (EarthLab), and the Marine Big Data Center of Institute for Advanced Ocean Study of Ocean University of China.

References

1. LRTAP Convention : Manual on Methodologies and Criteria for Modelling and Mapping Critical Loads & Levels and Air Pollution Effects, Risks and Trends. Chapter 3: Mapping Critical levels for Vegetation: UNECE Convention on Long-range Transboundary Air Pollution.; 2017. Available from: https://icpvegetation.ceh.ac.uk/get-involved/manuals/mapping-manual
2. Ainsworth EA. Understanding and improving global crop response to ozone pollution. *Plant Journal* 2017, **90**(5)**:** 886-897.
3. Musselman RC, Lefohn AS, Massman WJ, Heath RL. A critical review and analysis of the use of exposure- and flux-based ozone indices for predicting vegetation effects. *Atmospheric Environment* 2006, **40**(10)**:** 1869-1888.
4. Wilkinson S, Mills G, Illidge R, Davies WJ. How is ozone pollution reducing our food supply? *Journal of Experimental Botany* 2012, **63**(2)**:** 527-536.
5. United Nations. Transforming Our World: The 2030 Agenda for Sustainable Development. 2015 [cited]Available from: https://www.undp.org/sustainable-development-goals
6. FAOSTAT. The State of Food and Angriculture 2021. 2021 [cited]Available from: https://www.fao.org/state-of-food-security-nutrition/zh/
7. Clifton OE, Fiore AM*, et al.* Dry Deposition of Ozone Over Land: Processes, Measurement, and Modeling. *Reviews of Geophysics* 2020, **58**(1).
8. Agathokleous E, Kitao M, Kinose Y. A Review Study on Ozone Phytotoxicity Metrics for Setting Critical Levels in Asia. *Asian Journal of Atmospheric Environment* 2018, **12**(1)**:** 1-16.
9. Hoshika Y, Moura B, Paoletti E. Ozone risk assessment in three oak species as affected by soil water availability. *Environmental Science and Pollution Research* 2018, **25**(9)**:** 8125-8136.
10. Reich PB, Amundson RG. Ambient levels of ozone reduce net photosynthesis in tree and crop species. *Science (New York, NY)* 1985, **230**(4725)**:** 566-570.
11. Ronan AC, Ducker JA, Schnell JL, Holmes CD. Have improvements in ozone air quality reduced ozone uptake into plants? *Science of the Anthropocene* 2020, **8**(2).
12. Van Dingenen R, Dentener FJ*, et al.* The global impact of ozone on agricultural crop yields under current and future air quality legislation. *Atmospheric*

Environment 2009, **43**(3)**:** 604-618.

13. Fishman J, Creilson JK*, et al.* An investigation of widespread ozone damage to the soybean crop in the upper Midwest determined from ground-based and satellite measurements. *Atmospheric Environment* 2010, **44**(18)**:** 2248-2256.
14. Avnery S, Mauzerall DL, Liu J, Horowitz LW. Global crop yield reductions due to surface ozone exposure: 1. Year 2000 crop production losses and economic damage. *Atmospheric Environment* 2011, **45**(13)**:** 2284-2296.
15. Tai APK, Martin MV, Heald CL. Threat to future global food security from climate change and ozone air pollution. *Nature Climate Change* 2014, **4**(9)**:** 817-821.
16. Mills G, Sharps K*, et al.* Closing the global ozone yield gap: Quantification and cobenefits for multistress tolerance. *Global Change Biology* 2018, **24**(10)**:** 4869-4893.
17. Feng Z, De Marco A*, et al.* Economic losses due to ozone impacts on human health, forest productivity and crop yield across China. 2019, **131:** 104966.
18. Pei J, Liu P*, et al.* Estimating yield and economic losses induced by ozone exposure in South China based on full-coverage surface ozone reanalysis data and high-resolution rice maps. 2023, **13**(2)**:** 506.
19. Feng Z, Xu Y*, et al.* Ozone pollution threatens the production of major staple crops in East Asia. *Nature Food* 2022, **3**(1)**:** 47-56.
20. Avnery S, Mauzerall DL, Liu J, Horowitz LW. Global crop yield reductions due to surface ozone exposure: 2. Year 2030 potential crop production losses and economic damage under two scenarios of O_3 pollution. *Atmospheric Environment* 2011, **45**(13)**:** 2297-2309.
21. Lin M, Horowitz LW*, et al.* Vegetation feedbacks during drought exacerbate ozone air pollution extremes in Europe. *Nature Climate Change* 2020, **10**(5)**:** 444-+.
22. Xiao X, Xu Y*, et al.* Amplified Upward Trend of the Joint Occurrences of Heat and Ozone Extremes in China over 2013-20. *Bulletin of the American Meteorological Society* 2022, **103**(5)**:** E1330-E1342.
23. Schnell JL, Prather MJ. Co-occurrence of extremes in surface ozone, particulate matter, and temperature over eastern North America. *Proceedings of the National Academy of Sciences of the United States of America* 2017, **114**(11)**:** 2854-2859.
24. Hong C, Mueller ND*, et al.* Impacts of ozone and climate change on yields of perennial crops in California. *Nature Food* 2020, **1**(3).
25. Gao Y, Fu JS*, et al.* The impact of emission and climate change on ozone in the United States under representative concentration pathways (RCPs). *Atmospheric Chemistry and Physics* 2013, **13**(18)**:** 9607-9621.
26. Zhang J, Gao Y*, et al.* Impacts of compound extreme weather events on ozone in the present and future. *Atmospheric Chemistry and Physics* 2018, **18**(13)**:** 9861-9877.

27. Zhang J, Gao Y*, et al.* Isolating the modulation of mean warming and higher-order temperature changes on ozone in a changing climate over the contiguous United States. *Environmental Research Letters* 2022, **17**(9).

28. Zhang L, Gao Y*, et al.* Global impact of atmospheric arsenic on health risk: 2005 to 2015. *Proceedings of the National Academy of Sciences of the United States of America* 2020, **117**(25)**:** 13975-13982.

29. Ma M, Gao Y*, et al.* Substantial ozone enhancement over the North China Plain from increased biogenic emissions due to heat waves and land cover in summer 2017. *Atmospheric Chemistry and Physics* 2019, **19**(19)**:** 12195-12207.

30. Ashmore MR. Assessing the future global impacts of ozone on vegetation. *Plant Cell and Environment* 2005, **28**(8)**:** 949-964.

31. Fuhrer J. Introduction to the special issue on ozone risk analysis for vegetation in Europe. *Environmental Pollution* 2000, **109**(3)**:** 359-360.

32. Shang B, Agathokleous E*, et al.* Drought mitigates the adverse effects of O₃ on plant photosynthesis rather than growth: A global meta-analysis considering plant functional types. *Plant Cell and Environment* 2024.

33. Anav A, De Marco A*, et al.* Legislative and functional aspects of different metrics used for ozone risk assessment to forests. *Environmental Pollution* 2022, **295**.

34. Colette A, Tognet F*, et al.* Long-term evolution of the impacts of ozone air pollution on agricultural yields in Europe: a modelling analysis for the 1990-2010 period: European Topic Centre on Air Pollution and Climate Change Mitigation; 2018.

35. Pleijel H, Danielsson H, Broberg MC. Benefits of the Phytotoxic Ozone Dose (POD) index in dose-response functions for wheat yield loss. *Atmospheric Environment* 2022, **268:** 118797.

36. Bueker P, Feng Z*, et al.* New flux based dose-response relationships for ozone for European forest tree species. *Environmental Pollution* 2015, **206:** 163-174.

37. Pleijel H, Wallin G*, et al.* Ozone deposition to an oat crop (Avena sativa L.) grown in open-top chambers and in the ambient air. *Atmospheric Environment* 1994, **28**(12)**:** 1971-1979.

38. Ainsworth EA, Lemonnier P, Wedow JM. The influence of rising tropospheric carbon dioxide and ozone on plant productivity. *Plant Biology* 2020, **22:** 5-11.

39. Zhang J, Tang H, Liu G, Zhu J. Stomatal ozone flux-response relationships of rice(Oryza sativa L.)in subtropical area. *Journal of Agro-Environment Science* 2016, **35**(10)**:** 1857-1866.

40. Feng Z, Tang H*, et al.* A stomatal ozone flux-response relationship to assess ozone-induced yield loss of winter wheat in subtropical China. *Environmental Pollution* 2012, **164:** 16-23.

41. Peng J, Shang B*, et al.* Ozone exposure- and flux-yield response relationships for maize. *Environmental Pollution* 2019, **252:** 1-7.

42. Zhang W, Feng Z*, et al.* Quantification of ozone exposure- and stomatal uptake-

yield response relationships for soybean in Northeast China. *Science of the Total Environment* 2017, **599:** 710-720.

43. Zhao H, Chang J*, et al.* China's future food demand and its implications for trade and environment. *Nature Sustainability* 2021, **4**(12)**:** 1042-1051.

44. Cassman KG, Grassini P. A global perspective on sustainable intensification research. *Nature Sustainability* 2020, **3**(4)**:** 262-268.

45. Wang T, Xue L*, et al.* Ozone pollution in China: A review of concentrations, meteorological influences, chemical precursors, and effects. *Science of the Total Environment* 2017, **575:** 1582-1596.

46. Xu X, Lin W*, et al.* Long-term changes of regional ozone in China: implications for human health and ecosystem impacts. *Elementa-Science of the Anthropocene* 2020, **8**.

47. Lu X, Zhang L*, et al.* Rapid Increases in Warm-Season Surface Ozone and Resulting Health Impact in China Since 2013. *Environmental Science & Technology Letters* 2020, **7**(4)**:** 240-247.

48. Guo J ZX, Gao Y, Wang Z, Zhang M, Xue W, Herrmann H, Brasseur GP, Wang T, Wang Z. What Track Will It Follow? *Environ Sci Technol* 2023, **57**(1)**:** 109-117.

49. Meinshausen M, Nicholls ZRJ*, et al.* The shared socio-economic pathway (SSP) greenhouse gas concentrations and their extensions to 2500. *Geoscientific Model Development* 2020, **13**(8)**:** 3571-3605.

50. Kou W, Gao Y*, et al.* High downward surface solar radiation conducive to ozone pollution more frequent under global warming. *Science Bulletin* 2023, **68**(4)**:** 388-392.

51. Feng Z, Kobayashi K*, et al.* Impacts of current ozone pollution on wheat yield in China as estimated with observed ozone, meteorology and day of flowering. *ATMOSPHERIC ENVIRONMENT* 2019, **217**.

52. Wang Y, Wild O*, et al.* Reductions in crop yields across China from elevated ozone*. *Environmental Pollution* 2022, **292**.

53. Schauberger B, Rolinski S, Schaphoff S, Mueller C. Global historical soybean and wheat yield loss estimates from ozone pollution considering water and temperature as modifying effects. *Agricultural and Forest Meteorology* 2019, **265:** 1-15.

54. Sofiev M, Tuovinen J-PJAE. Factors determining the robustness of AOT40 and other ozone exposure indices. 2001, **35**(20)**:** 3521-3528.

55. Mills G, Buse A*, et al.* A synthesis of AOT40-based response functions and critical levels of ozone for agricultural and horticultural crops. *Atmospheric Environment* 2007, **41**(12)**:** 2630-2643.

56. Anav A, De Marco A*, et al.* Comparing concentration-based (AOT40) and stomatal uptake (PODY) metrics for ozone risk assessment to European forests. 2016, **22**(4)**:** 1608-1627.

57. Zhang J, Gao Y*, et al.* Disentangling the mechanism of temperature and water

vapor modulation on ozone under a warming climate. *Environmental Research Letters* 2022, **17**(12).

58. Sun J, Feng Z, Ort DR. Impacts of rising tropospheric ozone on photosynthesis and metabolite levels on field grown soybean. *Plant Science* 2014, **226:** 147-161.

59. Liu Z, Deng Z*, et al.* Challenges and opportunities for carbon neutrality in China. *Nature Reviews Earth & Environment* 2022, **3**(2)**:** 141-155.

60. Hu S, Zhang Y*, et al.* Challenges and opportunities for carbon neutrality in China's building sector-Modelling and data. *Building Simulation* 2022, **15**(11)**:** 1899-1921.

61. Vass MM. Renewable energies cannot compete with forest carbon sequestration to cost-efficiently meet the EU carbon target for 2050. *Renewable Energy* 2017, **107:** 164-180.

62. Jin L, Yi Y, Xu J. Forest carbon sequestration and China's potential: the rise of a nature-based solution for climate change mitigation. *China Economic Journal* 2020, **13**(2)**:** 200-222.

63. Gao Y, Zhang J*, et al.* Nonlinear effect of compound extreme weather events on ozone formation over the United States. *Weather and Climate Extremes* 2020, **30**.

64. Teskey R, Wertin T*, et al.* Responses of tree species to heat waves and extreme heat events. *Plant Cell and Environment* 2015, **38**(9)**:** 1699-1712.

65. Chen Z, Dayananda B*, et al.* Research on the Potential of Forestry's Carbon-Neutral Contribution in China from 2021 to 2060. *Sustainability* 2022, **14**(9).

66. Chen L, Msigwa G*, et al.* Strategies to achieve a carbon neutral society: a review. *Environmental Chemistry Letters* 2022, **20**(4)**:** 2277-2310.

67. Huang M-T, Zhai P-M. Achieving Paris Agreement temperature goals requires carbon neutrality by middle century with far-reaching transitions in the whole society. *Advances in Climate Change Research* 2021, **12**(2)**:** 281-286.

68. Plöchl M, Lyons T, Ollerenshaw J, Barnes J. Simulating ozone detoxification in the leaf apoplast through the direct reaction with ascorbate. *Planta* 2000, **210**(3)**:** 454-467.

69. Rai R, Agrawal M. Assessment of competitive ability of two Indian wheat cultivars under ambient O₃ at different developmental stages. *Environmental Science and Pollution Research* 2014, **21**(2)**:** 1039-1053.

70. Massman WJ. Toward an ozone standard to protect vegetation based on effective dose: a review of deposition resistances and a possible metric. *Atmospheric Environment* 2004, **38**(15)**:** 2323-2337.

71. Pleijel H, Danielsson H*, et al.* Growth stage dependence of the grain yield response to ozone in spring wheat (Triticum aestivum L.). *Agriculture Ecosystems & Environment* 1998, **70**(1)**:** 61-68.

72. Fu R, Shang B, Zhang G, Feng Z. Differential effects of ozone pollution on photosynthesis and growth of rice during two growth stages. *Journal of Agro-*

Environment Science 2021, **40**(10)**:** 2066-2075.

73. Wu R, Zheng Y, Hu C. Evaluation of the chronic efects of ozone on biomass loss of winter wheat based on ozone flux-response relationship with dynamical flux thresholds. *Atmospheric Environment* 2016, **142:** 93-103.

74. Emberson LD, Wieser G, Ashmore MR. Modelling of stomatal conductance and ozone flux of Norway spruce: comparison with field data. *Environmental Pollution* 2000, **109**(3)**:** 393-402.

75. Pleijel H, Danielsson H*, et al.* An ozone flux-response relationship for wheat. *Environmental Pollution* 2000, **109**(3)**:** 453-462.

76. Pleijel H, Danielsson H*, et al.* Ozone risk assessment for agricultural crops in Europe: Further development of stomatal flux and flux-response relationships for European wheat and potato. *Atmospheric Environment* 2007, **41**(14)**:** 3022-3040.

77. Danielsson H, Karlsson GP, Karlsson PE, Pleijel H. Ozone uptake modelling and flux-response relationships - an assessment of ozone-induced yield loss in spring wheat. *Atmospheric Environment* 2003, **37**(4)**:** 475-485.

78. Moore N, Alagarswamy G*, et al.* East African food security as influenced by future climate change and land use change at local to regional scales. *Climatic Change* 2012, **110**(3-4)**:** 823-844.

79. Feddema JJ, Oleson KW*, et al.* The importance of land-cover change in simulating future climates. *Science* 2005, **310**(5754)**:** 1674-1678.

80. Pielke RA, Marland G*, et al.* The influence of land-use change and landscape dynamics on the climate system: relevance to climate-change policy beyond the radiative effect of greenhouse gases. *Philosophical Transactions of the Royal Society of London Series a-Mathematical Physical and Engineering Sciences* 2002, **360**(1797)**:** 1705-1719.

81. Maynard K, Royer JF. Effects of "realistic" land-cover change on a greenhouse-warmed African climate. *Climate Dynamics* 2004, **22**(4)**:** 343-358.

82. Li Z, Molders N. Interaction of impacts of doubling CO₂ and changing regional land-cover on evaporation, precipitation, and runoff at global and regional scales. *International Journal of Climatology* 2008, **28**(12)**:** 1653-1679.

83. He C, Zhang J, Liu Z, Huang Q. Characteristics and progress of land use/cover change research during 1990-2018. *Journal of Geographical Sciences* 2022, **32**(3)**:** 537-559.

84. Chen M, Vernon CR*, et al.* Global land use for 2015-2100 at 0.05° resolution under diverse socioeconomic and climate scenarios. *Scientific Data* 2020, **7**(1).

85. Shoukat MR, Cai D*, et al.* Warming Climate and Elevated CO₂ Will Enhance Future Winter Wheat Yields in North China Region. *Atmosphere* 2022, **13**(8).

86. Zhao W, Chou J*, et al.* Impacts of Extreme Climate Events on Future Rice Yields in Global Major Rice-Producing Regions. *International Journal of*

Environmental Research and Public Health 2022, **19**(8).

87. Yang X, Chen F*, et al.* Potential benefits of climate change for crop productivity in China. *Agricultural and Forest Meteorology* 2015, **208:** 76-84.

88. Luo N, Meng Q*, et al.* China can be self-sufficient in maize production by 2030 with optimal crop management. *Nature Communications* 2023, **14**(1).

89. Gao Y, Fu JS*, et al.* Projected changes of extreme weather events in the eastern United States based on a high resolution climate modeling system. *Environmental Research Letters* 2012, **7**(4).

90. Zhang G, Gao Y*, et al.* Seesaw haze pollution in North China modulated by the sub-seasonal variability of atmospheric circulation. *Atmospheric Chemistry and Physics* 2019, **19**(1)**:** 565-576.

91. Yan F, Gao Y*, et al.* Revealing the modulation of boundary conditions and governing processes on ozone formation over northern China in June 2017. *Environmental Pollution* 2021, **272**.

92. Zeng X, Gao Y*, et al.* Characterizing the distinct modulation of future emissions on summer ozone concentrations between urban and rural areas over China. *Science of the Total Environment* 2022, **820**.

93. Hodges M, Belle JH*, et al.* Delays in reducing waterborne and water-related infectious diseases in China under climate change. *Nature Climate Change* 2014, **4**(12)**:** 1109-1115.

94. Wu D, Wang P*, et al.* Measured phenology response of unchanged crop varieties to long-term historical climate change. 2019, **13:** 47-58.

95. Zhang J, Chen S*, et al.* Review of vegetation phenology trends in China in a changing climate. 2022, **46**(6)**:** 829-845.

96. Xu Y, Kobayashi K, Feng Z. Wheat yield response to elevated O3 concentrations differs between the world's major producing regions. *Science of the Total Environment* 2024, **907**.

97. Broberg MC, Daun S, Pleijel H. Ozone Induced Loss of Seed Protein Accumulation Is Larger in Soybean than in Wheat and Rice. *Agronomy-Basel* 2020, **10**(3).

98. Wang X, Zhang D*, et al.* An Intermittent Exposure Regime Did Not Alter the Crop Yield and Biomass Responses to an Elevated Ozone Concentration. 2024, **15**(4)**:** 464.

99. Yarwood G, Whitten, G., Jung, J., Heo, G., and Allen, D. Development, evaluation and testing of version 6 of the carbon Bond chemical mechanism (CB6): ENVIRON International Corporation and Center for Energy and Environmental Resources of The University of Texas at Austin 2010b.

100. Appel KW, Napelenok, S., Hogrefe, C., Pouliot, G., Foley, K. M., Roselle, S. J., Pleim, J. E., Bash, J., Pye, H. O., and Heath, N. *Overview and evaluation of the community multiscale air quality (CMAQ) modeling system version 5.2.* Springer International Publishing AG, Cham (ZG): Switzerland, 2017.

101. Randerson JT, G.R. van der Werf, L. Giglio, G.J. Collatz, and P.S. Kasibhatla.

Global Fire Emissions Database, Version 4.1 (GFEDv4). In: DAAC O, editor. Oak Ridge, Tennessee, USA; 2018.

102. Liu H, Meng Z-H*, et al.* Emissions and health impacts from global shipping embodied in US-China bilateral trade. *Nature Sustainability* 2019, **2**(11)**:** 1027-1033.

103. Luo Y, Zhang Z*, et al.* ChinaCropPhen1km: a high-resolution crop phenological dataset for three staple crops in China during 2000-2015 based on leaf area index (LAI) products. *Earth System Science Data* 2020, **12**(1)**:** 197-214.

104. Liu Y, Dai L. Modelling the impacts of climate change and crop management measures on soybean phenology in China. *Journal of Cleaner Production* 2020, **262**.

105. Jarvis, P. G. The Interpretation of the Variations in Leaf Water Potential and Stomatal Conductance Found in Canopies in the Field. *Philosophical Transactions of the Royal Society of London* 1976, **273**(927)**:** 593-610.

106. Emberson L, Ashmore MR*, et al.* Modelling stomatal ozone flux across Europe. *Environmental Pollution* 2000, **109**(3)**:** 403-413.

107. Raschke K, Hanebuth WF, Farquhar GD. Relationship between stomatal conductance and light intensity in leaves of Zea mays L., derived from experiments using the mesophyll as shade. *Planta* 1978, **139**(1)**:** 73-77.

108. Lanoue J, Leonardos ED, Grodzinski B. Effects of Light Quality and Intensity on Diurnal Patterns and Rates of Photo-Assimilate Translocation and Transpiration in Tomato Leaves. *Frontiers in Plant Science* 2018, **9**.

109. Zhang Q, Peng S, Li Y. Increase rate of light-induced stomatal conductance is related to stomatal size in the genus <i>Oryza</i>. *Journal of Experimental Botany* 2019, **70**(19)**:** 5259-5269.

110. Urban J, Ingwers M, McGuire MA, Teskey RO. Stomatal conductance increases with rising temperature. *Plant Signaling & Behavior* 2017, **12**(8).

111. Huang G, Yang Y*, et al.* Temperature responses of photosynthesis and stomatal conductance in rice and wheat plants. *Agricultural and Forest Meteorology* 2021, **300**.

112. Zhao H, Zheng Y, Zhang Y, Li T. Evaluating the effects of surface O_3 on three main food crops across China during 2015-2018. *Environmental Pollution* 2020, **258**.

113. Lin Y, Jiang F*, et al.* Impacts of O_3 on premature mortality and crop yield loss across China. *Atmospheric Environment* 2018, **194:** 41-47.

114. Zhao H, Wang L*, et al.* Quantifying ecological and health risks of ground-level O_3 across China during the implementation of the "Three-year Action Plan for Cleaner Air". *Science of the Total Environment* 2022, **817**.

115. USEPA. Guidance on the Use of Models and Other Analyses for Demonstrating Attainment of Air Quality Goals for Ozone, PM2.5, and Regional Haze: US Environmental Protection Agency, Office of Air Quality Planning and Standards.; 2007.

116. Monfreda C, Ramankutty N, Foley JA. Farming the planet: 2. Geographic distribution of crop areas, yields, physiological types, and net primary production in the year 2000. *Global Biogeochemical Cycles* 2008, **22**(1).
117. Li DS, Drew; Ding, Dian; Lu, Xiao; Zhang, Lin; Zhang, Yuqiang Surface ozone impacts on major crop production in China from 2010 to 2017. *Atmospheric Chemistry and Physics Discussions* 2021**:** 1-23.
118. Tang H, Takigawa M*, et al.* A projection of ozone-induced wheat production loss in China and India for the years 2000 and 2020 with exposure-based and flux-based approaches. *Global Change Biology* 2013, **19**(9)**:** 2739-2752.
119. Dong Can GR, Zhang Xin, Li Hong, Wang Wenxing, Xue Likun. Assessment of O-3-induced crop yield losses in northern China during 2013-2018 using high-resolution air quality reanalysis data. *Atmospheric Environment* 2021, **259**.

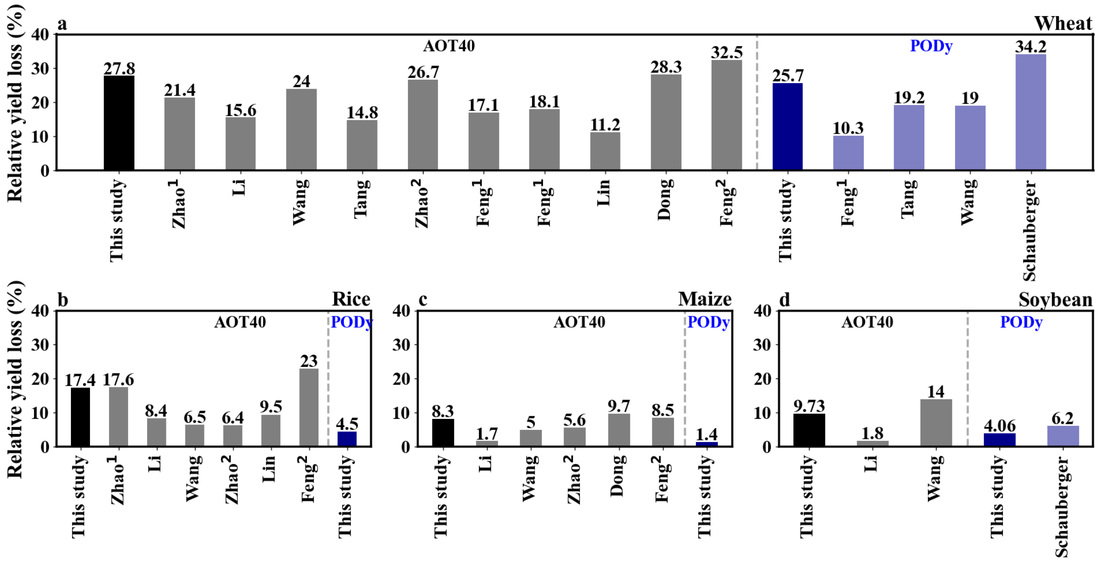

Fig. 1 | Annual relative yield loss from various of studies based on AOT40 (black bars) and PODy (blue bars) for wheat (a), rice (b), maize (c), and soybean (d) in China. Dark-colored bars represent the results of this study, while light-colored bars represent findings from other studies. The x-axis labels indicate previous studies: Zhao[1] (ref.[114]), Li[117], Wang[52], Tang[118], Zhao[2] (ref.[112]), Feng[1] (ref.[51]), Lin [113], Dong[119], Feng[2](ref.[19]), and Schauberger[53].

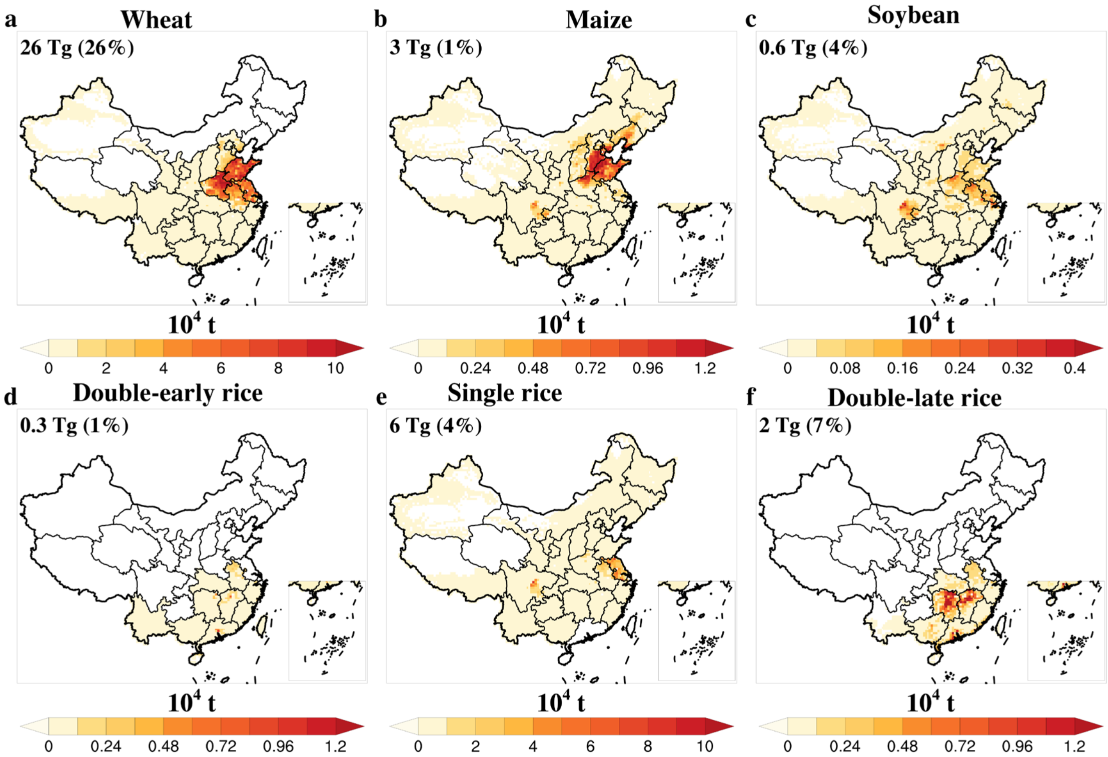

Fig. 2 | The spatial distribution of annual yield loss for wheat (a), maize (b), soybean (c), Double-early rice (d), Single-rice (e) and Double-late rice (f) during the historical period based on PODy. Blank areas across China represent regions without cultivation of these crops. The numbers in the top left corner of each panel indicate the total annual national losses, calculated by multiplying the relative yield loss by the total crop production. The national relative yield loss (shown in parentheses) is derived by dividing the total annual national losses by the total crop production, providing a percentage that reflects the proportion of yield loss at the national level.

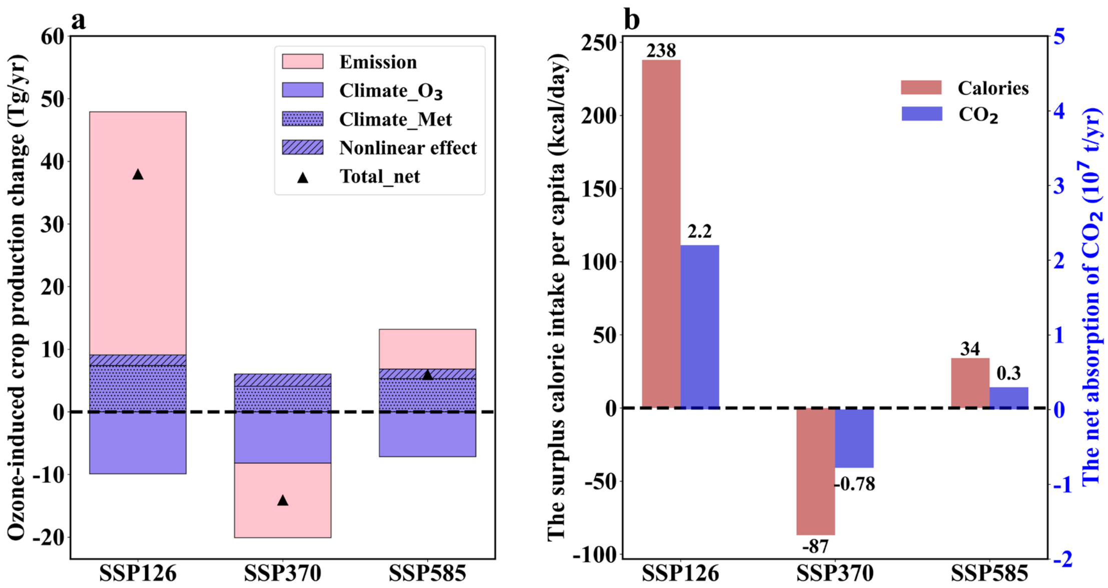

Fig. 3 | Future annual changes in ozone-induced crop production under SSP scenarios relative to the historical period (a), and the corresponding surplus calories and net CO_2 uptake (b). In (a), the pink and purple histograms represent the contributions of anthropogenic emissions and climate change, respectively, while the grey triangles indicate the net changes in crop production. These changes are shown relative to mid-century under the SSP scenarios. For the purple histograms, solid, dotted, and dashed patterns represent the contributions from ozone concentrations, meteorological conditions, and their synergistic effects, respectively.

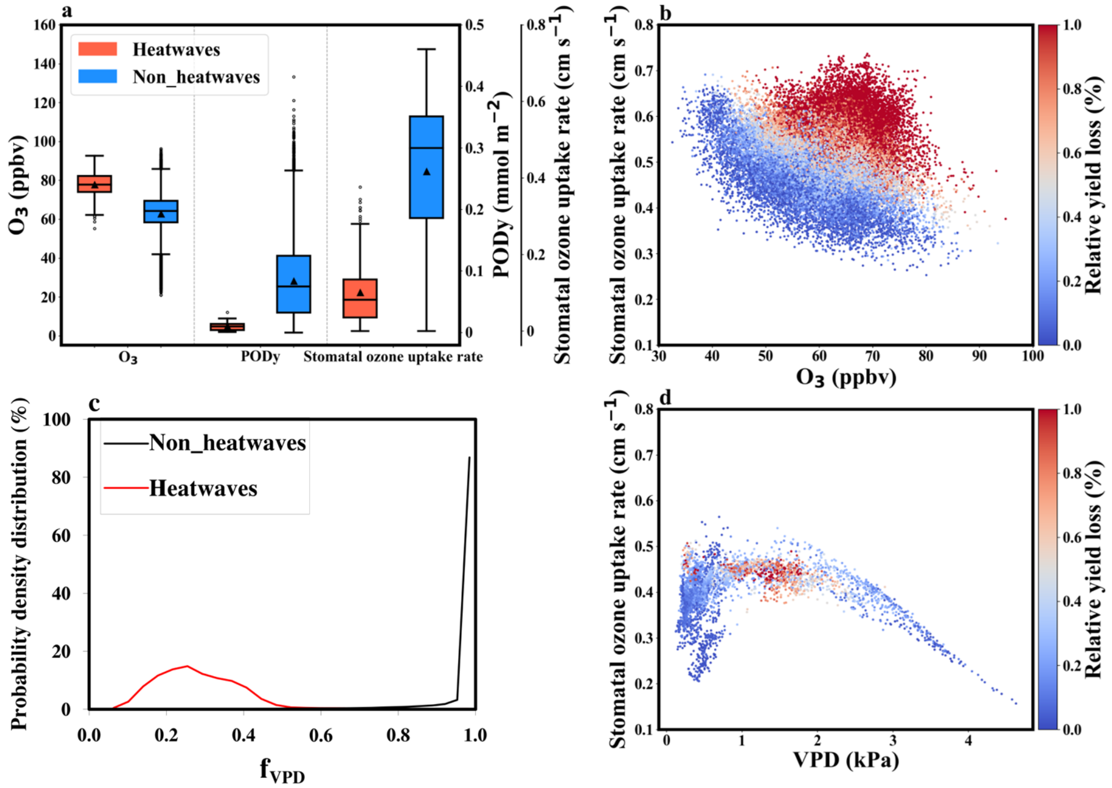

Fig. 4 | Comparison of daily ozone concentrations, PODy, stomatal ozone uptake rate, atmospheric water vapor pressure deficit (f_{VPD}) during heatwave and non_heatwave periods in the wheat phenological period from 2015 to 2019. (a) ozone concentration, PODy and stomatal ozone uptake rate during heatwave and non-heatwave periods, with the 25^{th} and 75^{th} percentile (boxes), interquartile range (difference between 75^{th} and 25^{th} percentile), medians (horizontal lines), means (black triangles) and endpoints indicating values 1.5 times the interquartile range above the upper and below the lower quartiles. All other values are considered outliers and are marked with hollow circles. (b) Variations in relative yield loss (%) as ozone concentration and stomatal ozone uptake rate change. (c) Probability density distribution of the daily f_{VPD} factor, which measures the limitation imposed by VPD on stomatal function. (d) Variations in stomatal ozone uptake rate and relative yield loss as VPD increases.

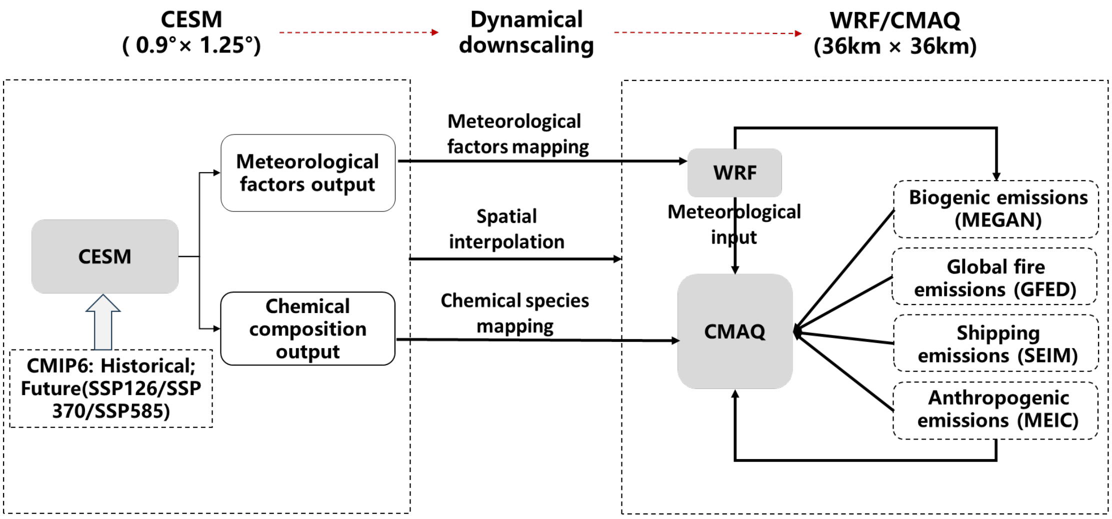

1003

1004 **Fig. 5 | The modeling system used in this study.**

1005

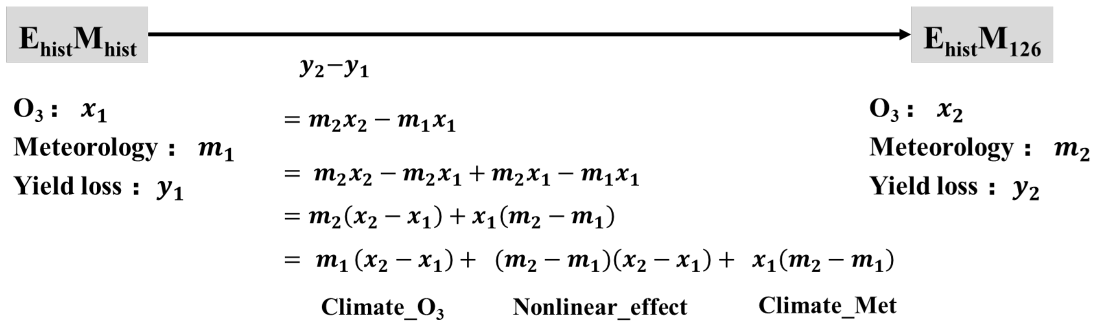

Fig. 6 Decomposition diagram illustrating the factors contributing to crop production losses. Shown are results due to changes in future weather conditions, using the SSP126 scenario with historical emissions as an example: $E_{hist}M_{126}$.